Mechanisms of the Anatomically Correct Testbed Hand

Ashish D. Deshpande, Zhe Xu, Michael J. Vande Weghe, Benjamin H. Brown, Jonathan Ko, Lillian Y. Chang, David D. Wilkinson, Sean M. Bidic, and Yoky Matsuoka

***Abstract*—We have built an anatomically correct testbed (ACT) hand with the purpose of understanding the intrinsic biomechanical and control features in human hands that are critical for achieving robust, versatile, and dexterous movements, as well as rich object and world exploration. By mimicking the underlying mechanics and controls of the human hand in a hardware platform, our goal is to achieve previously unmatched grasping and manipulation skills. In this paper, the novel constituting mechanisms, unique muscle to joint relationships, and movement demonstrations of the thumb, index finger, middle finger, and wrist of the ACT Hand are presented. The grasping and manipulation abilities of the ACT Hand are also illustrated. The fully functional ACT Hand platform allows for the possibility to design and experiment with novel control algorithms leading to a deeper understanding of human dexterity.**

***Index Terms*—Biomimetics, movement control, muscle moment arms, robotic hands.**

I. Introduction

HUMAN hands can perform many dexterous grasping and manipulation tasks. Hand *dexterity* is the ability to precisely control movements and forces using all of the hand's degrees of freedom (DOFs) to perform a variety of tasks. Examples include the ability to play musical instruments, use chopsticks, gesture, and perform daily tasks, such as cooking and writing.

Researchers have been designing robotic hands for more than four decades [36], [52], [55], and while many advancements have been made in the newer robotic hands, the grasping and manipulation abilities of the current robotic hands do not match the versatile dexterity of the human hand. Most of the existing robotic hands are designed to meet a narrow set of task requirements, e.g., prosthetic robot hands are designed to achieve basic grasping with low-weight mechanisms, while hands for industrial applications are designed to handle specific parts. Striving for human-like capabilities, current robotic hands have been designed to be anthropomorphic, having fingers and an opposable thumb with human-like shapes and DOFs. However, the actual mechanisms of actuation and controls, in most cases, have not been anatomical in these prostheses. This is in part due to lack of clear understanding of biomechanical features of the human hand and also due to the difficulty in translating human features to a machine form.

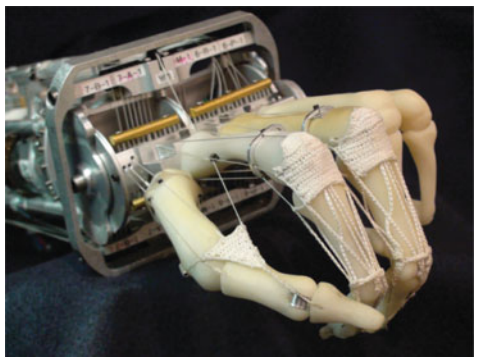

Fig. 1. Anatomically correct testbed hand.

Versatile and robust dexterity are achieved in the human hand through a combination of hand biomechanics, which can be thought as the 'hardware', and neural controls, which can be thought as the 'software' of the hand. To design a robotic hand that achieves human-like dexterity, we have embarked upon a distinct approach toward robotic hand design. We have constructed the anatomically correct testbed (ACT) hand, as shown in Fig. 1 in which the mechanical elements are designed to mimic the intricate features of hand biomechanics, including bone structures and tendon arrangements, and the software controls are based on the human-hand neuromuscular control system. With these attributes, the ACT Hand opens up the hitherto unavailable possibility of addressing critical design questions about human-hand functionality.

Our long-term goals are to achieve human-like dexterity in robotic form and to enhance the understanding of human-hand functionality through experiments with the developed robotic platform. Toward these goals, we have accomplished a critical

Manuscript received October 22, 2010; revised January 29, 2011 and May 13, 2011; accepted July 25, 2011. Date of publication October 3, 2011; date of current version September 12, 2012. A. D. Deshpande, Z. Xu, and M. J. Vande Weghe contributed equally as first authors. Recommended by Technical Editor J. Ueda.

A. D. Deshpande is with the Department of Mechanical Engineering, University of Texas, Austin, TX 78712 USA (e-mail: ashish.deshpande@maine.edu).

Z. Xu and Y. Matsuoka are with the Department of Computer Science and Engineering, University of Washington, Seattle, WA 98195 USA (e-mail: zhexu@cs.washington.edu; yoky@cs.washington.edu).

M. J. V. Weghe and B. H. Brown are with The Robotics Institute, Carnegie Mellon University, Pittsburgh, PA 15213 USA (e-mail: vandeweg@cmu.edu; hbb@cs.cmu.edu).

J. Ko is with Google, Inc., Seattle, WA 98103 USA (e-mail: jonko@cs.washington.edu).

L. Y. Chang is with Intel Corporation, at the Intel Science and Technology Center at the University of Washington, and also with the Department of Computer Science and Engineering, University of Washington, Seattle, WA 98195 USA.

D. D. Wilkinson is with Barrett Technology, Inc., Cambridge, MA 02138 USA (e-mail: wilkdave@gmail.com).

S. M. Bidic is with the UT Southwestern Clinical Procedure Center, Dallas, TX 75390 USA (e-mail: sean@bidic.org).

Color versions of one or more of the figures in this paper are available online at http://ieeexplore.ieee.org.

Digital Object Identifier 10.1109/TMECH.2011.2166801

step, which is the development of a robotic hand with mechanical parts that closely imitate the biomechanical features of the human hand. Previous researchers have attempted to develop an understanding of human hand biomechanics and controls by either conducting experiments with cadaver hands, or by developing computational models of hand biomechanics and movements. However, since the most critical human-hand features are exposed only through dynamic physical interactions with objects, and since the nonlinear interactions between the muscles, tendons, bones, and joints are extremely challenging to recreate in computational models, a physical realization—in the form of a detailed anatomical model—is necessary to define and analyze the human-hand features. None of the existing hands are designed to possess the hardware and software intricacies to tackle the important research questions about dexterity of hands, while the ACT Hand has the potential to achieve human-like muscle control.

The purpose of this paper is to present our novel ideas for the constituting mechanisms and to summarize the developments and results in the ACT Hand design. One key advantage of human-like mechanisms is that the robotic hand possesses nonlinear, nonconstant relationships between the actuators (*muscles*), and joints. We develop mathematical models for these relations based on the data collected from experiments with the ACT Hand. We demonstrate that the moment arm variations match with the known relations in the human hand. Moreover, our model is more comprehensive than the existing models for the human hand, thus leading to a better understanding of human-hand biomechanics. The moment arm relations are key for achieving reliable position control of the digits of the ACT Hand. We present results from position tracking of the index finger and thumb in Section V.

II. Related Work

Robotic hands have been developed for many decades for a variety of applications ranging from industrial manufacturing to prosthetics to humanoid robot research. Although numerous grasping and manipulation results have been demonstrated by existing anthropomorphic hands (e.g., fast manipulation by the hand developed by the University of Tokyo [58]), the capabilities of the current robotic hands do not match the abilities of the human hand. Design of a versatile and robust robotic hand that demonstrates human-like grasping and manipulation capacity is a challenging task. The design decisions include the number of fingers, number of joints, DOFs, range of motion (ROM) for the joints, speed of movements, and force generation capacity. The design choices have to be made under tight space and weight constraints. Focus has been on increasing the number of DOFs, adding sensors, and implementing novel controls, including machine learning methods. Table I presents a list of representative robotic hands with important characteristics of these hands. Note that in many of cases, the robotic hands are still under development, so the grasping and manipulation abilities are based on the design specification and not from actual demonstrations.

Many robotic hands are driven directly or through gears, e.g., the Stanford/JPL Hand [55], Barrett Hand [65], the Southampton Hand [43], the Gifu Hand II [39], the NASA/JPL Robonaut Hand [11], the NAIST hand [68], and the high-speed hand from the University of Tokyo [58]. (The drive mechanisms for the recently developed DEKA arm–hand prosthesis [24] have not been published.) Examples of tendon-driven hands include: the Okada Hand [52], the Utah/MIT Hand [30], [36], [62], the DLR II Hand [44], the UB Hand 3 [46], the Vanderbilt Hand [22], the CyberHand [15], the Karlsruhe Hand [37], [65], the smart motor and air muscle Shadow Hands [59], and the Keio Hand [74].

The idea of designing smart mechanisms to simplify controls has been explored in some of the existing hands. For example, in the underactuated grippers, such as the SDM Hand [28] and SPRING Hand [17], joint compliance is implemented to be able to conform to different shapes for grasping with relatively simple controls. Some researchers have developed soft skin to accommodate against errors and to embed sensors [8], [57]. However, the ability of these hands to execute human-level manipulation tasks remains limited.

Despite the desire for dexterity in prosthetics, the most commonly used prosthetic hand is a mechanically controlled hook prosthesis [35], which was designed over a century ago. Several researchers [16], [22], [51] and companies [48], [53], [64] have designed robotic hands specifically for prosthetic purposes with attention toward minimizing weight, simplifying controls, and aesthetics. Some of the current commercial prostheses are controlled by means of electromyographic (EMG) signals recorded using surface electrodes, which detect electrical activity related to the patient's arm muscles [53], [64]. Because of the difficulty in translating the user intent into useful controls signals, current prosthetic hands have only one or two DOFs, thus leading to limited functionality. Some surveys reveal that 30–50% of the upper extremity amputees do not use their prosthetic hand regularly because of reduced functionality, poor cosmetic appearance, and limited controllability [3], [16], [60]. Ideas for controlling of robotic hands using neural signals have also been explored. Recent studies enable monkeys to control the 3-D movement of a robotic arm to achieve self-feeding tasks [50], [70]. Over 30 human arm/hand amputees have received nerve reinnervation surgery to rewire the peripheral nerves that used to go into the hand/arm to the chest muscle instead [41]. The signals amplified by the natural muscle can then be tapped into with surface EMG for prosthetic arm/hand control.

A number of researchers have developed computational models of hand biomechanics [25], [34]. While some of the recent models do include human-like muscles, tendons, and bones [34], [63], [66], these models still face difficulties in simulating critical nonlinear relationships, e.g., tendons sliding over bones, and nonlinear joint movements. For instance, Sueda *et al.* present an automatic technique for generating the motion of tendons and muscles [63], and Tsang *et al.* present an anatomically accurate inverse dynamics of the hand [66]. However, these methods do not represent the nonlinear moment arm relationships for the hand muscle, which are critical in defining biomechanics of the hand. Considering the challenges in modeling nonlinear relations and advantages gained through experiments with physical

TABLE I
FEATURES OF EXEMPLARY ROBOTIC HANDS

Robotic hands	*# identical fingers*	*# joints / DOF (Total DOFs)*[1]	*Range of motion*	*Speed of motion*	*Activation / transmission method*	*Types of grasps / manipulation*
Hosmer hook [35]	2 split hooks	1/1 (1 DOF)	<human hand	<human hand	body-powered	splitting hook pinch
Utah Arm / Liberating / OttoBock [48], [45], [53]	2	T-1/1, I-1/0, M-1/0 (1 DOF)	<human hand	<human hand	EMG signal driven, DC motor, cable	three-finger pinch
USC/Belgrade [7]	4	T-3/2, I-3/0.5, M-3/0.5, R-3/0.5, P-3/0.5 (4 DOFs)	<human hand	<human hand	DC motor, cable, linkage	grasp: power & finger tip
Harvard SDM [29]	4	4×2/1 (1 DOF)	>human hand	<human hand	DC motor, cable, elastic joints	enveloping grasp
Gatech Dusty [73]	1	2/1 (1 DOF)	<human hand	–	DC motor, cable, spring hinge joints	nonprehensile grasp
Barrett [65]	3	T(Right)-2/1.5, T(Left)-2/1.5, I-2/1 (4 DOFs)	>human hand	≈1.2×human hand	DC motor, worm drives integrated with cable drive and breakaway clutch	grasp: power & finger tip
i-Limb [64]	4	T-3/1, I-2/1, M-2/1, R-2/1, P-2/1 (5 DOFs)	<human hand	≈human hand	DC motors, belt transmission	grip: key, hook, power & precision; grasp: spherical & palmar
Southampton [43]	4	T-2/2, I-3/1, M-3/1, R-3/1, P-3/1 (6 DOFs)	<human hand	≈0.22×human hand	DC motor, worm-wheel, lead screw	power grasp, lateral pinch
Cyber [15]	5	T-4/2, I-3/1, M-3/1, R-3/1, P-3/1 (6 DOFs)	≈0.22×human hand	≈0.38×human hand	geared DC motor, lead screw, cable, exensor spring	lateral pinch; grasp: cylindrical, spherical & tripod
Univ. of Tokyo Hand [58]	3	T(R)-3/3, I-2/2, T(L)-3/3 (8 DOFs)	>human hand	=15×human hand	DC motor, harmonic and bevel gear transmission	grasp: power & finger tip; dynamic manipulation
Stanford/JPL [55]	3	T-3/3, I-3/3, M-3/3 (9 DOFs)	>human hand	—	DC motor, cable	finger tip grasp
DARPA hand [23]	4	T-3/3, I-3/2, M-3/2, R-3/2, P-3/2 (11 DOFs)	<human hand	<human hand	DC motor, cable, gear transmission	grasp: hook & power
Robonaut [47]	4	T-5/3, I-4/3, M-4/3, R-3/3, P-3/1 (11 DOFs)	≈human hand	<human hand	DC motor, flex shaft, lead screw, cable	grasp: power & finger tip; lateral pinch
Naist [68]	4	T-4/3, I-4/3, M-4/3, R-4/3 (12 DOFs)	≈human hand	≈human hand	geared DC motor, bevel gear	power grasp
DLR II [14]	4	T-4/4, I-4/3, M-4/3, R-4/3 (13 DOFs)	>human hand	=3×human hand	DC motor, belt, harmonic drive, bevel gears	grasp: power & finger tip; lateral pinch
Utah/MIT [36]	4	T-4/4, I-4/4, M-4/4, R-4/4 (16 DOFs)	<human hand	≈1.82×human hand	pneumatic actuator, cable	finger tip grasp /manipulation
Gifu III [49]	4	T-4/4, I-4/3, M-4/3, R-4/3, P-4/3 (16 DOFs)	≈human hand	≈1.35×human hand	DC motor, gear transmission, linkage mechanism	power grasp
UB III [46]	4	T-3/4, I-4/4, M-4/3, R-4/2, P-4/3 (16 DOFs)	<human hand	≈0.51×human hand	DC motor, cable, helical spring	grasp: power & finger tip
Shadow [59]	4	T-5/5, I-4/3, M-4/3, R-4/3, P-4/3 (17 DOFs)	≈human hand	≈0.5×human hand	air muscle, cable and spring	grasp: finger tip & power
Keio [74]	4	T-4/4, I-4/4, M-4/4, R-4/4, P-4/4 (20 DOFs)	≈human hand	≈2×human hand	ultrasonic motors, elastic elements, cable	grasp: power & finger tip; lateral pinch

[1]T, I, M, R, and P denote thumb, index, middle, ring, and little finger, respectively.

prototypes, we believe that it is important to continue developing both computational and physical models of human hand.

To improve the performance and capabilities of the robotic hands, new ideas have to be introduced for both the robot hardware and controls. Robotics researchers can greatly benefit from a better understanding of the biomechanics and neuromuscular controls of the human hand. Although many robotic hands are designed to be anthropomorphic, the intrinsic mechanisms of actuation and controls, in most cases, have not been anatomical. In this context, the ACT Hand is designed to be a tool to investigate human dexterity. By incorporating the biomechanical features of the human hand, the ACT Hand allows for the identification of the critical factors that lead to dexterity in the human hand.

TABLE II
ACT HAND PHALANGE LENGTHS

Finger	*Phalange*	*Length (cm)*
Index	MCP to PIP	5.10
	PIP to DIP	2.69
	Distal phalange	1.55
Middle	MCP to PIP	5.38
	PIP to DIP	3.58
	Distal phalange	1.80
Thumb	CMC Flex to CMC Ab-Ad	2.31
	CMC Ab-Ad to MCP	4.31
	MCP to PIP	3.65
	Distal phalange	2.00

III. ACT HAND MECHANISMS

This section describes the mechanical design and fabrication details of the ACT Hand. Overall, the focus is on mimicking the intrinsic biomechanics, actuation, and control behavior to achieve human-like dynamic movements, rather than minimizing the total weight of the hand. The following sections describe the mechanical components in the ACT Hand, including its finger bones, joints, tendons, and actuators.

A. ACT Hand Finger Bones

In an early version of the ACT Hand, the fingers were designed with cylindrical bones [72] with the assumption that a biological tendon arrangement would lead to anatomical performance even with engineering shapes for the bones. However, experiments with this design revealed that the biological shapes of the human finger bones create moment arms for the tendons that vary with joint angle, a behavior critical for accurate hand function [1], [2], [18], [69]. The variable moment arms are necessary for achieving human-like joint-muscle movement relationships. The mass and inertial properties of the bones also affect the dynamic behavior of the fingers. To address these issues, we designed the finger bones by accurately matching the size, shape, and mass properties of human bones. We used Stratasys Corporation's existing laser-scan model of human left-hand bones supplied in the STL format, imported the tessellate facets into Pro/Engineer, and created solid models for each bone by fitting new surfaces to the scan geometry. The lengths of the phalanges are given in Table II.

The composition of the finger bones was designed with two primary goals in mind: ease of manufacturing the complex surface shapes, and high strength at the joints and tendon attachment points. An earlier version of the ACT Hand utilized cast aluminum and 7075 aluminum bones, which were difficult to fabricate and offered only moderate strength, especially, to hold the small threaded fasteners used at the tendon insertion points. The current version uses innovative design with two separate components. The core of the bones is comprised of a set of steel beams, which offers superior strength and durability, and although not easy to machine, the beams are much more straightforward to fabricate than the complex surface shapes in the previous design. Attached to the beams are outer plastic shells fabricated using stereolithography. Because the shells are only used in compression in our application the strength provided by the plastic material is sufficient. The stereolithography manufacturing process makes it easy to experiment with modified surface geometries and replace the shells when they wear out or break.

B. ACT Hand Finger Joints

The design of the finger joints plays a critical role in matching ACT Hand kinematics with human kinematics. The locations of the DOF and axes of rotations and the ROMs for all the finger joints are debated in the biomechanics literature. In the ACT Hand, we have mimicked the most broadly accepted biomechanical model of DOF and ROM for the fingers [13], [32], [33]. All fingers have four DOFs, while the opposable thumb has five nonorthogonal, nonintersecting DOFs. The base of the ring and little fingers in the palm has additional DOFs.

Thumb, index, and middle fingers are actuated by anatomically routed tendons and muscle-equivalent actuators. All fingers can hyperextend, similar to the human fingers. We chose to defer the completion of actuation for the last two fingers until we investigate the performance of multifinger object manipulations with three fingers. The wrist has two DOFs, and all finger tendons are routed with moment arms preserved, i.e., wrist movements influence finger movements, as for humans.

In the first version of the ACT Hand, joint design was based on human joint biomechanics—ligaments connect bones and create a joint capsule filled with cartilage and synovial fluid to achieve a low-friction joint [10]. Although mimicking joint geometry yielded accurate motion vectors, it resulted in high-friction and reduced ROM. In the current design, we implemented the joints as machined pin joints and sought to align the joint axes to best approximate the more complex motion of each human finger joint. In some cases, we discovered that joints, which at the first glance might appear to be 3-DOF ball-and-socket joints, were actually better represented by two carefully aligned pin joints. Figs. 2 and 3 show the CAD models for the index finger and thumb.

1) Index and Middle Finger Joints: There are three joints in the index and middle fingers, namely, the metacarpophalangeal (MCP), proximal interphalangeal (PIP), and distal interphalangeal (DIP). These are modeled by a novel design involving pin joints in the ACT Hand. The PIP joint is located at the distal end of the proximal phalangeal bone and the DIP joint is located at the distal end of the middle phalangeal bone. The MCP joint has two DOFs: one to achieve flexion–extension (FE) and another to realize abduction–adduction (AA) finger motion. These two DOFs are realized by a gimbal mechanism at the distal end of the MCP bone. To match the anatomical joint properties of the human index finger, as described in [12], the AA joint axis is oriented at 60° with respect to the MCP bone as shown in Fig. 2.

2) Thumb Joints: The three thumb joints are the carpometacarpal (CMC), MCP, and IP joints. The IP joint possesses

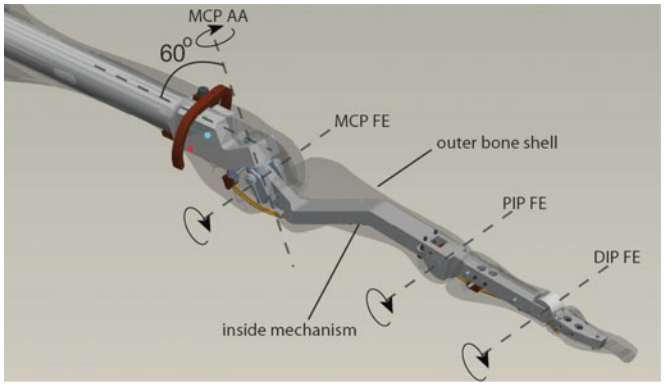

Fig. 2. ACT Hand index finger bones are made up of two materials. The outer shell, made up of plastic, matches the human shape and size, while the inner steel beam structure allows for anatomical joints.

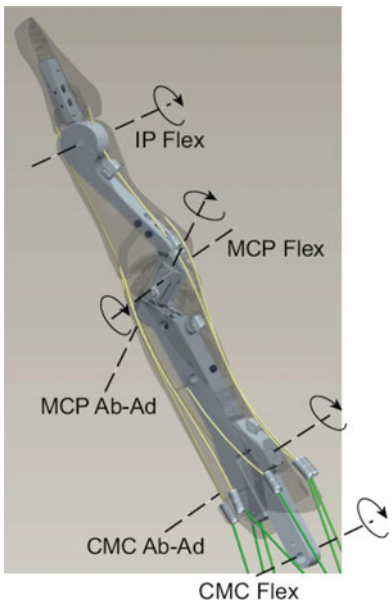

Fig. 3. Bones and joints in the thumb of the ACT thumb. The thumb has three joints, namely, the CMC, MCP, and IP, and five DOFs.

one rotation DOF in the FE direction. The DOF and joint axes locations for the CMC and MCP joints are debated in hand-biomechanics research. Recent research shows that defining two DOFs with two nonintersecting, nonorthogonal axes [32], [33], [56], [61] instead of one universal joint at each of these joints [21], [38] leads to more anatomically correct thumb behavior. In the ACT Hand, the two DOFs at the CMC joint are realized by two nonperpendicular, nonintersecting pin joints, and the two DOFs at the MCP joint are realized by a gimbal mechanism, as shown in Fig. 3. Supported by a pair of miniature ball bearings, the gimbal piece rotates around the MCP AA axis fixed within the metacarpal bone. A small pin joint in the gimbal piece represents the MCP FE axis, which is fixed relative to the proximal phalange via a link arm. The sweep of the joint cavity restricts the movement of the gimbal assembly to the appropriate MCP joint ROM.

The CMC joint involves two pin joints at the ends of a single-link arm to realize the AA and FE DOFs. Though the CMC and MCP joints are conceptually similar in that they both have FE and AA DOFs, a gimbal design is not suitable for the CMC joint because its two rotational axes are located in separate bones. One pin joint coincides with the CMC AA axis in the proximal end of the metacarpal, while the other pin joint represents the CMC FE axis, which intersects the trapezium carpal bone. Joint ROM for each of the two axes is constrained by narrow slot cuts in the metacarpal and trapezium bones. The IP joint design consists of a single pin joint to represent the FE DOF between the two phalangeal bones. A link arm rigidly attached to the distal phalange rotates about an axle coinciding with the IP FE axis in the proximal phalange. The geometry of the articulating bone ends was maintained except for a narrow slot that allows the small-diameter link arm to rotate around the IP FE axis pin. The span of the cavity enforces the joint ROM.

TABLE III
ACT HAND FINGER JOINT MOTION LIMITS

Finger	*Joint*	*Minimum*	*Maximum*
Index	MCP	30° extension	90° flexion
		35° abduction	35° adduction
	PIP	0° extension	110° flexion
	DIP	0° extension	70° flexion
Middle	MCP	30° extension	90° flexion
		35° abduction	35° adduction
	PIP	0° extension	110° flexion
	DIP	0° extension	70° flexion
Thumb	CMC	40° extension	40° flexion
		40° abduction	40° adduction
	MCP	60° extension	60° flexion
		15° abduction	15° adduction
	IP	20° extension	80° flexion

3) Joint ROM: Joint limits for the flexion joints are imposed by creating internal beam features that interfere with one another at the limits. The ROMs were chosen to match those of the human finger and are shown in Table III. Because the gimbals used for the MCP joints are free to rotate by $\pm 180^{\circ}$, we designed the bone shells to limit the ROM by contacting each other at the joint limits. For example, Fig. 2 shows the CAD model of the MCP joint of the ACT Hand's index finger with the bone shell around the gimbal joint to ensure the correct ROM.

C. ACT Hand Tendons

Two types of muscles control hand movements: 1) those located in the palm, called the *intrinsic muscles* and 2) those located in the forearm, called the *extrinsic muscles*. The muscles are connected to the bones by long tendons that pass over the joints, terminating at the insertion points on the finger bones. Muscle contractions lead to hand movement and force generation. In the ACT Hand, we used brushless DC motors (described later in the text) as muscles and we fabricated our tendons with 0.46 mm Spectra(R) strings. The string was chosen because of its strength (200-N breaking strength), stiffness (4800 N/strain), and ability to slide smoothly over the bones. The tendons in the

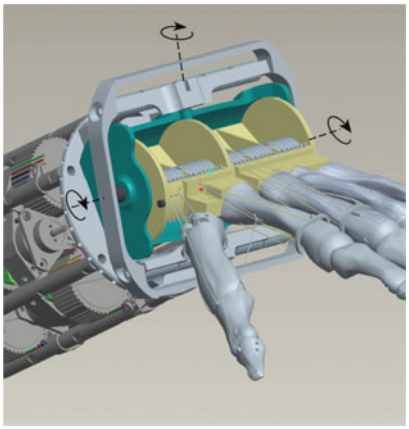

Fig. 4. Wrist joint mechanism with two DOFs.

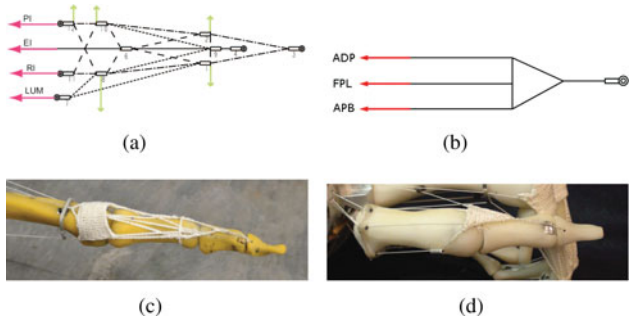

Fig. 5. Tendon hood structure for the index finger and thumb. (a), (b) Schematic. (c), (d) Actual.

human hand have elastic properties [75], which play a critical role in the hand dexterity and controls. The choice of a string with high stiffness allows for reliable and quantifiable relationships between the motors and joints. Mimicking the stiffness properties of the human tendons, either through hardware or software controls is part of our future work.

1) Tendon Routing Over the Wrist Joint: The human wrist position affects finger-joint properties (e.g., joint stiffness) because the tendons connecting the extrinsic muscles to the fingers travel past the wrist joint, and the joint position changes their path lengths. While designing the wrist for the ACT Hand, we faced a tradeoff of minimizing tendon friction versus routing tendons to be accurately affected by the wrist position. We chose to reduce tendon friction and explicitly designed a routing to minimize the effect of wrist position on tendon length. As shown in Fig. 4, each tendon crosses the wrist joint via a pair of sheaves—a large central sheave near the FE axis and a smaller outer sheave. The size and placement of the tendon sheaves have been chosen so that during wrist FE, the tendons unwind from one sheave as they are being wound onto the other, minimizing any change in path length. Wrist AA has a greater effect on path length due to the line of central sheaves rotating out of the plane of the outer sheaves, but the effect is small, particularly for tendons routed near the AA pivot point. Since the tension in each tendon is under independent software control, it is possible to undo the AA effects and apply the desired FE effects as a function of the wrist position.

2) Extensor Tendon Hood: On the dorsal side of the fingers, the tendons are connected from the bone insertion points to the actuators via an elaborate extensor tendon web. These networks of tendons play a central role in defining the biomechanics and control of the digits [1], [12]. To closely match the moment arm variations in the human hand, we developed a web of tendons that mimics the human structure with the spectra strings. The current version of the extensor mechanism is fabricated by crocheting nylon composite to emulate the geometry and functionality of the human counterpart as closely as possible as shown in Fig. 5. We prioritized our tendon structure design to achieve any posture that a typical human finger can achieve, mimic the overall geometry based on [31], produce a smooth surface to facilitate a sliding motion, and match the stiffness of a real tendon. The critical features of the extensor tendon web are the insertion points, the lateral bands and the hood, as shown in Fig. 5.

We have mimicked the exact locations of the bone insertion points in our tendon arrangements. The lateral bands serve the following functions: 1) assist lateral movements via the interosseous muscles when these muscles are activated as antagonists, 2) allow the extension of the distal phalanx and the finger as a whole when the interosseous muscles are activated as agonists in concert with the EDC muscle, and 3) coordinate the two distal joints (DIP and PIP) in FE [72]. The hood structure enables the flexion of the MCP joint independent of other joints and rotation at the MCP joint [72].

3) Flexor Side: The tendons on the flexion side are connected directly from the bone insertion points to the actuators. For example, notice the tendon routing in the flexion side of the thumb in Fig. 3. The flexion tendons pass through guiding "rockers" that allow for smooth travel of the tendon, while holding it close to the bone forms in order to achieve accurate moment arm lengths about the finger joints.

D. ACT Hand Actuators

The ACT Hand possesses the same number of muscles as the human hand: the index and middle fingers each have six muscles, namely, EI, RI, PI, LUM, FDS, and FDP, and the thumb has eight muscles, namely, EPL, EPB, APB, APL, OP, ADP, FPB, and FPL [13]. The wrist is actuated by four muscles. All muscles are realized by brushless DC motors located in the forearm. The tendon strings are wound on the threaded motor shaft, and the loose end is secured by a pin and knot arrangement, as shown in Fig. 6. The string–motor arrangement leads to matching the musculotendon property of one-dimensional (1-D) actuation, i.e., the muscles can only actuate by contraction. We investigated the possibility of using a direct linear muscle-like actuator, such as a shape memory alloy [42], McKibben muscles [71], or other artificial muscles [67]. However, none of these actuators can provide the fast response time ($<$200 ms), total excursion lengths ($>$4 cm), and possibility of variable stiffness that a human muscle can produce. At this stage of the ACT Hand's design, our focus is on mimicking the static and dynamic force and movement generation capacity, rather than the shape,

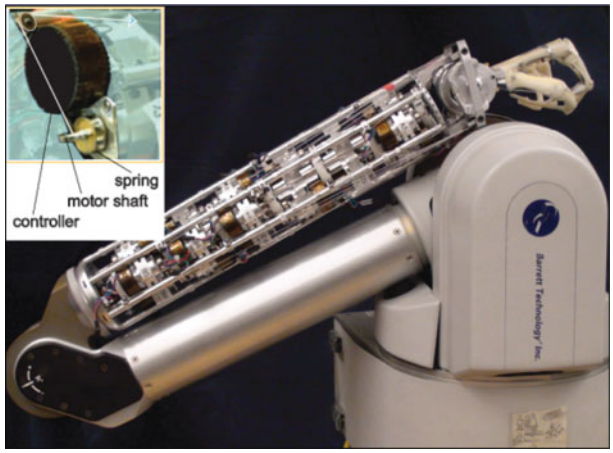

Fig. 6. ACT hand actuators arranged in the forearm.

size, or weight of the real muscle. Hence the choice of DC motors as actuators is justifiable. To overcome the torque ripple in the DC motors, we custom designed the DC motors[1] based on the Kollmorgen motor [40] as follows.

1) Magnet Skewing: One of the known issues with the permanent magnet DC motors is the motor cogging, which shows up as torque ripple at very low speeds [9]. The cogging effects can lead to errors in finger positions and jerky finger motions, especially during low-speed operations. To address this, we designed a rotor with permanent magnets cut into three pieces, longitudinally, which are staggered at 10° axial rotation with respect to each other. This method, called *step skewing* of the magnet, is a known, low-cost way to reduce the cogging torques [9]. The magnet skewing reduced the cogging torque to less than 30% of the original value, while the peak torque reduced by only 5%.

2) Motor Controller: Each motor is connected to a brushless servo controller (called the Puck [6]). Each controller has an embedded photosensor and an encoder wheel (with 114 ticks/degree) that allows for a high-precision position sensing of the motor rotation to mimic muscle spindles (see Fig. 6). The controllers are connected to an RTAI Linux [54] machine, which provides motor position readings at high frequency (>500 Hz).

3) Motor Housing in the Forearm: All motors are located in the forearm, as shown in Fig. 6. The motors are arranged in clusters of six units, and six clusters are connected end-to-end. The modular design of the clusters and motor housings allow for any motor to be easily replaced and entire clusters to be added or removed to match the number of actuators required for a particular setup. Additionally, the clusters incorporate guiding sheaves to route the tendon strings from their radial orientation after leaving the motor shaft to an axial orientation to reach the wrist.

[1]The brushless DC motor properties are: length 3 cm, outside radius 2.2 cm, peak torque 40 mN·m, stall torque 40 mN·m, torque constant 0.13 mN·m/A, and rise time 0.1 s.

E. Mounting the Hand onto an Arm

Since our focus is on understanding the movements of the hand and fingers, we mimicked the anatomy of the fingers and palm. Our wrist design is not anatomical in that it does not match the bone shapes and joint axes of the human wrist. However, we mimicked its FE and AA motions.

The wrist has two DoFs: a "yaw" joint ($\pm 15^\circ$) attached to the end of the arm, and a "pitch" joint ($\pm 30^\circ$) connected to the hand. Three banks of pulleys are mounted on the gimbal structure joining the two DOFs and guide the tendons from the arm-mounted actuators to the finger joints. These pulleys minimize friction in the tendon paths and route the tendons near the pitch axis to mimic the kinematic coupling present in a human hand. As explained earlier, all ACT Hand actuators are located in the forearm. The forearm and hand are mounted on a Whole Arm Manipulator (WAM) developed by Barrett Technologies, Inc. [6]. The WAM is a 4-DOF, cable-driven backdrivable manipulator. Its DC motor control allows position and force control modes. The ACT Hand forearm is connected to the WAM at the elbow joint using the same physical connection that connects the WAM forearm. Fig. 6 shows the entire assembly.

IV. Muscle-Joint Mappings: Moment Arms

An important characteristic of the human hand is the mechanical advantage, called the *moment arm*, that each muscle–tendon combination has on each joint. The muscle moment arms in the human hand are configuration dependent and play a critical role in hand-movement control; however, the exact properties of the moment arm variations are not known. Because the ACT Hand mimics hand biomechanics, through bone shapes and tendon hood structure, its muscle moment arms are also configuration dependent and determining the exact moment arm relationships is critical for ACT hand controls. Also, determination of the moment arm relationships in the ACT Hand can potentially lead to a better understanding of human-hand biomechanics.

We developed a method to acquire the moment arm relationships for the ACT Hand that is based on an analysis of motion capture data for finger and muscle–motor movements [26]. What follows are sample results from the moment arm analysis for the index finger of the ACT Hand. To determine the moment arms, we moved the index finger through its joint ROM and recorded the joint angles and changes in muscle lengths. We then found a functional mapping f_i among all four joint angles and each muscle excursion using a Gaussian process (GP)-based regression model

$$l_i = f_i(\overline{\theta}), \qquad i = 1, \ldots, 6 \tag{1}$$

where l_i is the excursion length for the muscle i, which is a member of the vector of muscle excursions ($\overline{l} = [l_1, l_2, l_3, l_4, l_5, l_6]^T$) and $\overline{\theta}$ is a vector of finger joint angles ($\overline{\theta} = [\theta_1, \theta_2, \theta_3, \theta_4]^T$). We define θ_1—MCP AA; θ_2–MCP FE; θ_3–PIP FE; and θ_4–DIP FE, with abduction and flexion as positive directions. The moment arm relationships were determined by taking the partial derivatives of the muscle-excursion functional mappings with respect to the joint angles. In the case of the ACT Hand index finger,

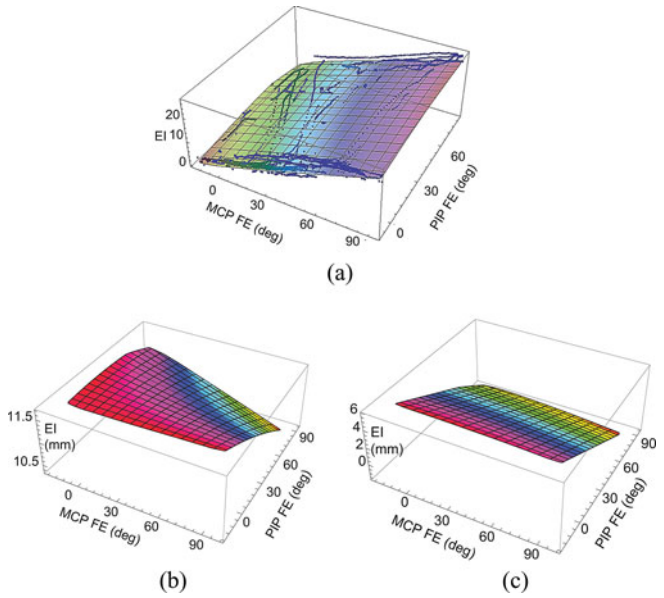

Fig. 7. Muscle excursions and moment arm variations for the EI muscle with respect to the MCP and PIP FE, as MCP flexion and PIP angles change. (a) EI excursions. (b) Variations in the EI moment arm w.r.t. MCP flex. (c) Variations in the EI moment arm w.r.t. PIP flex.

the moment arm is defined by a matrix R of dimension 6×4

$$\dot{\bar{l}} = R(\bar{\theta})\dot{\bar{\theta}} \tag{2}$$

where

$$R_{ij}(\bar{\theta}) = \frac{\partial l_i}{\partial \theta_j} = \frac{\partial f_i}{\partial \theta_j}, \quad i = 1, \ldots, 6 \quad \text{and} \quad j = 1, \ldots, 4. \tag{3}$$

Fig. 7(a) shows the variations in the excursions of EI muscles as two finger angles vary. The dots in the figure are the data points and the surfaces show the fitted mapping functions. Fig. 7(b) shows the variations in the moment arm of the EI muscle with respect to (w.r.t.) the MCP flex angle and Fig. 7(c) shows the variations in the moment arm of the EI muscle w.r.t. the PIP angle.

The mean error across all data points with the GP-based mapping is 0.65 mm (sd 0.33 mm). This error is low when compared with the total excursions, which are in the range of 30–40 mm. Our results show that the excursion lengths and moment arms for all muscles of the index finger depend significantly on all the joint positions of the finger.

A. Validation

We conducted experiments to test the quality of the angle to muscle-length mapping determined by our method. Fig. 8 shows the mapped muscle length when it was projected to the EI muscle length estimation. Table IV shows the mean absolute error for all muscle-length excursions when tested on a dataset of over 200 000 angles and muscle-length combinations. The data cover the physiological ROMs for all the finger joints. The actual excursion length was recorded directly from the encoder values, and the other estimations were from the joint angle information from a motion capture system translated to muscle lengths. We

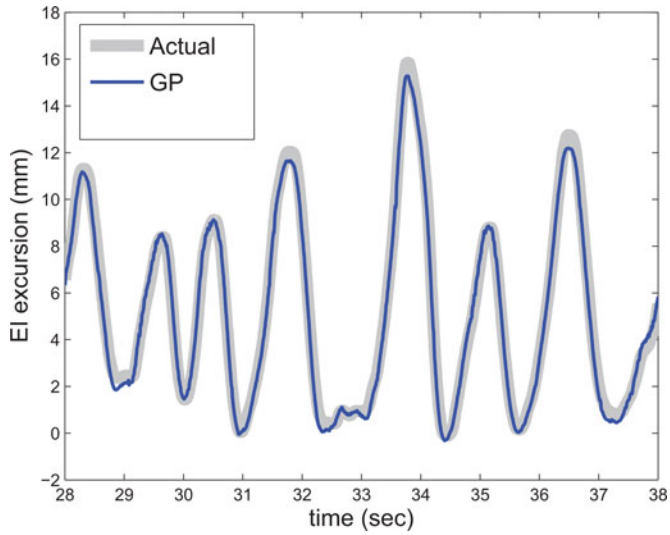

Fig. 8. Actual versus estimated length changes in the EI muscle during a typical finger motion.

TABLE IV
MEAN ABSOLUTE ERRORS IN MUSCLE TO JOINT MAPPINGS (MM)

	EI	*PI*	*FDP*	*LUM*	*FDS*	*RI*
error	0.1838	0.4193	0.1350	0.3192	0.1408	0.4567

used an optical motion-tracking system (Vicon 360 with six M2 cameras) to record motions of the finger involving all four joint angles. Thirteen markers, each 3 mm in diameter were placed on the ACT finger and the distribution of the markers was as follows: five on the MCP bone, three on the proximal and middle phalange, and two on the distal phalange. The *XYZ* positions of the markers were recorded at 120 Hz, and finger joint angles were determined by using an angle-determination algorithm built into the motion analysis software (Vicon iQ 2.5).

B. Comparison With Cadaver Data

We compare our results with index finger cadaver data from [1], where some of the most comprehensive datasets are available. To make the comparison we generated slice plots from our data by varying one angle at a time while keeping other joint angles constant as was done for generating the cadaver data. The moment arm values are higher in our case by 125% on average due to the fact that we modeled the ACT Hand size after a male subject and data in [1] as collected from a female specimen. A comparison between the ACT Hand moment arms and scaled human moment arms (by 125%) gives an overall mean error 3 ± 1.5 mm. The sign of moment arms, indicating contribution to FE or AA, for all muscles, except for LUM in parts of finger flexion, matches with the cadaver plots. Table V gives the correlation coefficients between individual muscle plots for MCP AA and FE variations. The first row gives the moment arms w.r.t. MCP flexion angle and the second row gives the moment arm w.r.t. MCP AA angle. The differences in variations in LUM and RI with the flexion angle and PI with adduction might have arisen due to the differences in the structure of LUM in the

TABLE V
CORRELATION COEFFICIENTS BETWEEN MOMENT ARM CURVES FROM THE CADAVER AND ACT HAND

	EI	*PI*	*FDP*	*LUM*	*FDS*	*RI*
MCP FE	0.94	0.47	0.83	-0.71	0.85	-0.95
MCP AA	0.99	-0.66	0.99	0.67	0.93	0.99

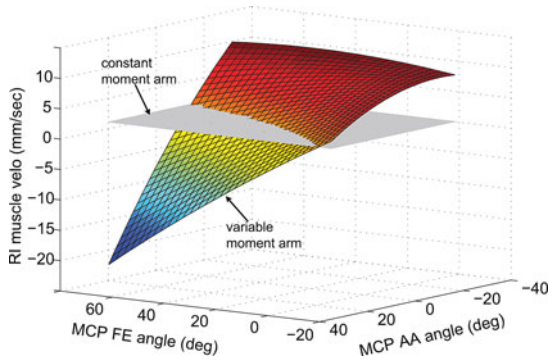

Fig. 9. Variations in muscle excursion velocity of RI as for constant joint-angle velocities with a variable moment arm and with a constant moment arm.

cadaver hands and the ACT Hand. The ACT lumbrical tendon and associated motor are attached to the equivalent of a skeletal anchor point. In contrast, the lumbrical tendon and associated muscle in human hands are attached to another sliding tendon.

C. Physical Interpretation of Moment Arm Variations

The extrinsic muscle excursions show significant dependence on flexion but little variation with adduction. In contrast, the intrinsic muscle excursions show significant dependence on both flexion and abduction. This means that the moment arms for all the muscles of the index finger depend significantly on all the joint positions of the finger and, for some of the muscles, the moment arms change sign. A negative value for the moment arm of a muscle with respect to a joint indicates that the muscle is contracting for positive change in the joint angle, meaning that the muscle actively contributes to joint movement. Conversely, a positive value for the moment arm means that the muscle is stretched for positive change in the joint angle. The moment arms for the muscle with respect to the primary angles show large variations and maintain the sign of the moment arms.

Our analysis leads to a mathematical model of the variations in the index finger moment arms when multiple joint move simultaneously. Since the ACT Hand structures imitate human anatomy, the moment arm variations provide insight into the human moment arm properties. Previous studies have analyzed moment arm variations with respect to motions of only one joint at a time. Also, our study analyzes moment arm variation with respect all four joints of the index finger, which is missing in the previous studies that focused only on the two MCP joints of the index finger. Thus, using the ACT Hand, we have determined previously unknown moment arm relationships in the human index finger.

Variable moment arms play a significant role in the movement control of the finger. For example, Fig. 9 shows a plot of variations in the muscle-excursion velocity of RI for the same angular velocities of MCP AA (0.5 rad/s), MCP FE (1.0 rad/s), PIP FE (1.0 rad/s), and DIP FE (1.0 rad/s). As the MCP AA and PIP FE angles vary, while MCP FE and DIP FE are kept constant, the RI velocity changes from positive to negative. This means that the muscle switched from being active and pulling to being passive and stretching. The figure also shows that a constant moment arm model, assumed in all the previous hand biomechanics studies, does not capture the variations in muscle velocities as functions of the finger configuration. Thus, to control the finger-joint velocities, muscle velocities should be generated based on the finger configuration using the variable moment arms. A constant moment arms assumption will lead to erroneous model of neuromuscular controls.

V. GRASPING AND HAND-MOVEMENT ILLUSTRATION

Taking advantage of the DOFs and ROMs in the ACT Hand, that are copied from the human hand, the ACT Hand is able to grasp and manipulate a number of objects that are part of daily activities. Fig. 10 shows nine examples of object grasping using the ACT Hand. These pictures demonstrate the DOFs and ROMs of the finger joints and the overall anthropomorphic grasping abilities. These nine objects were chosen to demonstrate the wide variety of grasps that can be achieved with the ACT Hand, e.g., power grasp in the case of the water bottle and pinch grasp in the case of the spoon. Grasping performance is greatly affected by the object interactions through skin contact. Currently, we are developing tactile skin for the ACT Hand.

These grasps were achieved through a direct muscle-control scheme [27]. For each grasp, we started from a neutral position of thumb, index finger, and middle finger, such that all fingers are open, and precalculated the joint angles for the specific grasp. The joint angles for the grasps were calculated by manually moving the fingers and recording the joint angles using the optical motion-tracking system (Vicon 360 with six M2 cameras). We, then, calculated the muscle excursions, i.e., contraction and stretch, necessary to achieve the desired joint angle and implemented position-integration control on the DC motor driving the muscle. Fig. 11 shows the changes in lengths for the thumb and index-finger muscles during the key grasp maneuver shown in Fig. 10. The top figure shows the muscle excursions for the six index-finger muscles and the bottom figure shows the muscle excursions for the eight thumb muscles. For the starting neutral position, the muscle excursions start at close to zero. Negative excursion means the muscle is contracting and positive excursion means that the muscle is stretching. As the finger joints flex, the flexors are contracted and extensors are stretched for both the thumb and the index finger. Notice that the muscle lengths change smoothly over the maneuver leading to smooth motions of the fingers. The mean tracking error over all muscles is 1.67 mm (sd 0.34 mm).

Considering that thumb movements account for more than 50% of the hand function [20], we also implemented a thumb movement of rubbing against the index finger, which is part of many daily hand movements, such as counting money and opening a plastic bag. Because of the mimicking of human

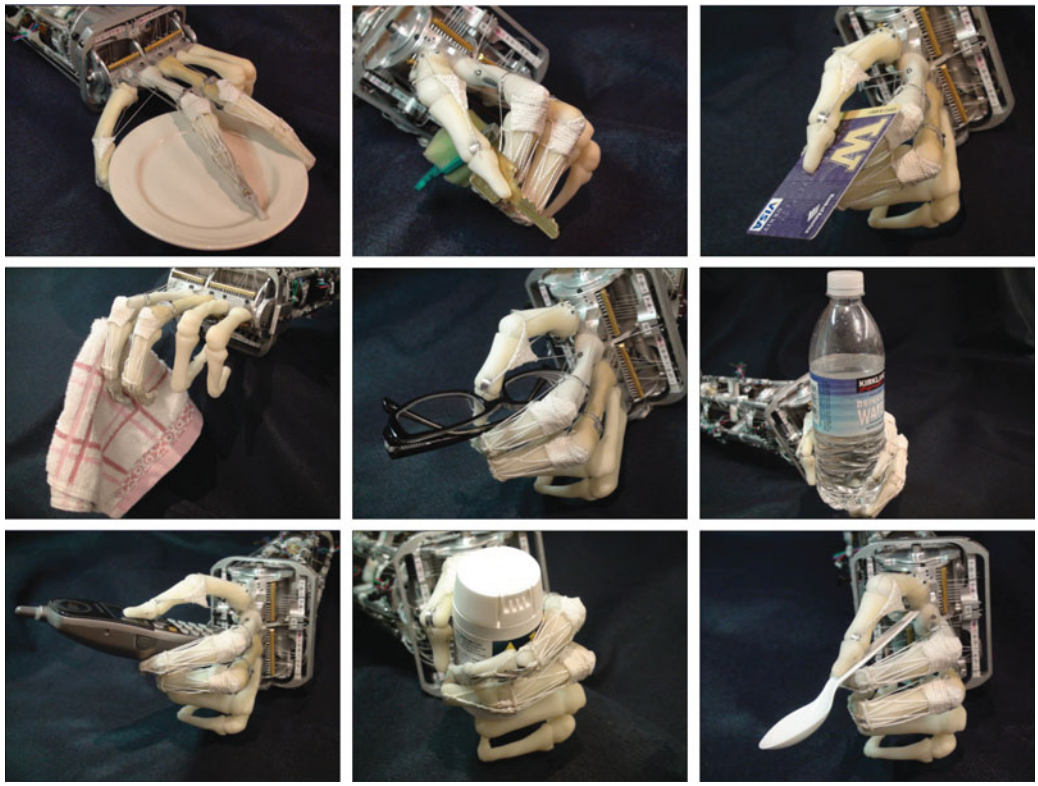

Fig. 10. ACT hand can grasp everyday objects with human-like finger postures. Figures show grasping of nine objects, namely, a coffee plate, key, credit card, hand towel, glasses, water bottle, cordless phone, medicine bottle, and spoon, which are identified as important for ALS patients [19].

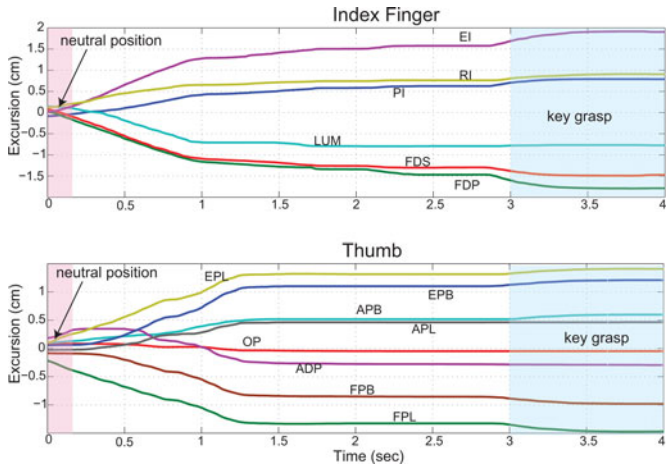

Fig. 11. Length changes in thumb and index-finger muscles during key grasp maneuver starting from neutral position (fingers open).

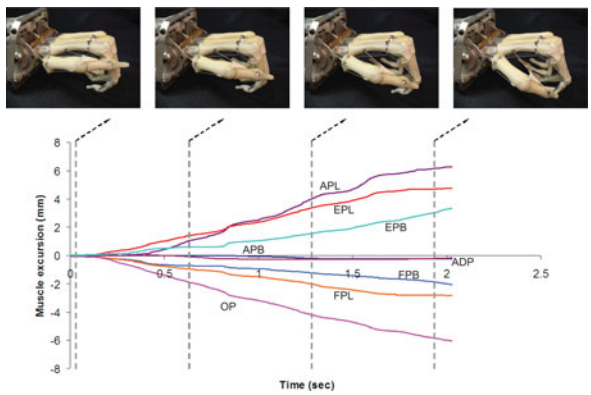

Fig. 12. With the anatomical DOFs, the thumb in the ACT Hand can be moved to rub the side of the index finger, which is a common and useful human motion. (Top) Sequence of photos taken at different times (dotted lines) during the movement execution. (Bottom) Plots of length changes (in mm) in the eight muscles of the thumb during this movement.

thumb biomechanics in the ACT Hand, including axes locations, number of DOFs, and muscle arrangements, we were able to generate an AA motion at the MCP joint in the ACT Hand thumb. Fig. 12 shows the snapshots of the thumb motion and corresponding length changes of the eight muscles during this motion.

VI. Conclusion and Future Work

This paper presents the novel constituting mechanisms, unique muscle-to-joint relations, and movement demonstrations of the thumb, index finger, middle finger, and wrist of the ACT Hand. The ACT Hand is designed to further our understanding of human-hand mechanisms and control and to provide guidelines for building versatile prosthetic and dexterous hands. We reviewed the state-of-the-art robotic hands and demonstrated that the unique design goals and features distinguish the ACT Hand when compared to the existing robotic hands. In Section III, we have presented a number of novel mechanical elements, which are designed and built to mimic human-hand biomechanics. These include the bone structures, joints, tendon arrangements,

and actuators in the fingers and thumb, and also the tendon routing and actuation of the wrist.

With the anatomically-correct mechanical elements, the ACT Hand uniquely mimics the human-hand biomechanics. We have carried out a data-driven kinematic analysis of the relationships between the muscles and joints, defined by the moment arms. Our analysis shows that the values for the moment arms for the muscles in the ACT Hand vary with the configuration of the hand, and these variations match the available data on human-hand biomechanics. Our model for moment arm variation is more comprehensive than the existing models for the human hand, thus leading to a better understanding of human-hand biomechanics. Development of tactile skin and passive joint properties in the ACT Hand are part of ongoing research.

Completion of the ACT Hand mechanisms and software platform allows us to conduct many experiments, which were hitherto impossible, to study human-hand properties and allows translation of important properties into robotic forms. For example, now we can implement novel control algorithms to develop a deeper understanding of human dexterity. Our group has investigated the existence and importance of muscle synergies during hand movement and force control [4], [5], and we are implementing these strategies in the ACT Hand. We are also investigating control strategies for achieving neuromuscular control of ACT Hand muscles [27]. We are planning to develop replicas of the ACT Hand and make them available for other researchers. This will allow for the simultaneous experimentation and growth in understanding of human-hand complexities.

REFERENCES

[1] K. N. An, Y. Ueba, E. Y. Chao, W. P. Cooney, and R. I. Linscheid, "Tendon excursion and moment arm of index finger muscles," *J. Biomech.*, vol. 16, pp. 419–425, 1983.

[2] K.-N. An, "Tendon excursion and gliding: Clinical impacts from humble concepts," *J. Biomech.*, vol. 40, pp. 713–718, 2007.

[3] D. J. Atkins, D. C. Heard, and W. Donovan, "Epidemiologic overview of individuals with upper limb loss and their reported research priorities," *Int. J. Prosthetics Orthotics*, vol. 8, pp. 747–761, 1996.

[4] R. Balasubramanian and Y. Matsuoka, "Biological stiffness control strategies for the anatomically correct testbed (ACT) hand," in *Proc. IEEE Int. Conf. Robot. Autom.*, 2008, pp. 737–742.

[5] R. Balasubramanian and Y. Matsuoka, "The role of small redundant actuators in precise manipulation," in *Proc. IEEE Int. Conf. Robot. Autom.*, 2009, pp. 4409–4415.

[6] Barrett Technology, Inc. (2009, Sep.). WAM specifications. [Online]. Available: http://www.barrett.com/robot/products-arm-specifications.htm

[7] G. Bekey, R. R. Tomovic, and I. Zeljkovic, "Control architecture for the belgrade/USC hand," *Dextrous Robot Hands.*, Berlin, Germany: Springer-Verlag, 1990.

[8] L. Biagiotti, P. Tiezzi, Vassura, and C. G. Melchiorri, *Modelling and Controlling the Compliance of a Robotic Hand With Soft Finger Pads*. (Springer Tracts in Advanced Robotics), F. Barbagli, D. Prattichizzo, and K. Salisbury, Eds. Berlin, Germany: Springer-Verlag, 2005.

[9] N. Bianchi and S. Bolognani, "Design techniques for reducing the cogging torque in surface-mounted PM motors," *IEEE Trans. Ind. Appl.*, vol. 38, no. 5, pp. 1259–1265, Sep./Oct. 2002.

[10] S. Bidic, J. Imbriglia, and Y. Matsuoka, "An anatomical hand for instruction and simulation," presented at the Amer. Soc. Surgery Hand Meeting, Chicago, IL, 2003.

[11] W. Bluethmann, R. Ambrose, M. Diftler, S. Askew, E. Huber, M. Goza, F. Rehnmark, C. Lovchik, and D. Magruder, "Robonaut: A robot designed to work with humans in space," *Auton. Robots*, vol. 14, pp. 179–197, 2003.

[12] P. W. Brand and A. M. Hollister, *Clinical Mechanics of the Hand*, 3rd ed. St. Louis, MO: Mosby, 1999.

[13] P. W. Brand and M. H. Anne, *Clinical Mechanics of the Hand*. St. Louis, MO: Mosby, 1993.

[14] J. Butterfass, M. Fischer, M. Grebenstein, S. Haidacher, and G. Hirzinger, "Design and experiences with DLR hand: II," in *Proc. World Autom. Congr.*, 28 Jun.–Jul. 1, 2004, vol. 15, pp. 105–110.

[15] M. C. Carrozza, G. Cappiello, S. Micera, B. B. Edin, L. Beccai, and C. Cipriani, "Design of a cybernetic hand for perception and action," *Biol. Cyben.*, vol. 95, no. 6, pp. 629–644, 2006.

[16] M. C. Carrozza, B. Massa, S. Micera, R. Lazzarini, M. Zecca, and P. Dario, "The development of a novel prosthetic hand: Ongoing research and preliminary results," *IEEE/ASME Trans. Mechatronics*, vol. 7, no. 2, pp. 108–114, Jun. 2002.

[17] M. C. Carrozza, C. Suppo, F. Sebastiani, B. Massa, F. Vecchi, R. Lazzarini, M. R. Cutkosky, and P. Dario, "The spring hand: Development of a self-adaptive prosthesis for restoring natural grasping," *Auton. Robots*, vol. 16, no. 2, pp. 125–141, 2004.

[18] L. Y. Chang and Y. Matsuoka, "A kinematic thumb model for the ACT hand," in *Proc. IEEE Int. Conf. Robot. Autom.*, 2006, pp. 1000–1005.

[19] Y. S. Choi, T. Deyle, and C. C. Kemp, "Benchmarking assistive mobile manipulation: A list of household objects for robotic retrieval prioritized by people with ALS," in *Proc. IEEE Int. Conf. Rehabil. Robot.*, 2009, pp. 510–517.

[20] J. C. Colditz, "Anatomic considerations for splinting the thumb," in *Rehabilitation of the Hand: Surgery and Therapy*, J. M. Hunter, E. J. MacKin, A. D. Callahan, Eds. Philadelphia, PA: Mosby, 2005.

[21] W. P. Cooney, M. J. E. Lucca, Y. Chao, and R. L. Linscheid, "The kinesiology of the thumb trapeziometacarpal joint," *J. Bone Joint Surg. Am.*, vol. 63, pp. 1371–1381, 1981.

[22] S. A. Dalley, T. E. Wiste, T. J. Withrow, and M. Goldfarb, "Design of a multifunctional anthropomorphic prosthetic hand with extrinsic actuation," *IEEE-ASME Trans. Mechatronics*, vol. 14, no. 6, pp. 699–706, Dec. 2009.

[23] DEKA. (2008). [Online]. Available: http://www.dekaresearch.com

[24] DEKA-HAND. (2010). Dean Kamen Luke arm prosthesis. [Online]. Available: http://www.dekaresearch.com/index.shtml

[25] S. Delp and J. Loan, "A graphics-based software system to develop and analyze models of musculoskeletal structures," *Comput. Biol. Med.*, vol. 25, no. 1, pp. 21–34, 1995.

[26] A. D. Deshpande, R. Balasubramanian, J. Ko, and Y. Matsuoka, "Acquiring variable moment arms for index finger using a robotic testbed," *IEEE Trans. Biomed. Eng.*, vol. 57, no. 8, pp. 2034–2044, 2010.

[27] A. Deshpande, J. Ko, D. Fox, and Y. Matsuoka, "Anatomically correct testbed hand control: Muscle and joint control strategies," in *Proc. IEEE Int. Conf. Robot. Autom.*, 2009, pp. 4416–4422.

[28] A. M. Dollar and R. D. Howe, "A robust compliant grasper via shape deposition manufacturing," *IEEE/ASME Trans. Mechatronics*, vol. 11, no. 2, pp. 154–161, Apr. 2006.

[29] A. Dollar and R. Howe, "Simple, robust autonomous grasping in unstructured environments," in *Proc IEEE Int. Conf. Robot. Autom.*, Apr. 2007, pp. 4693–4700.

[30] K. A. Farry, I. D. Walker, and R. G. Baraniuk, "Myoelectric teleoperation of a complex robotic hand," *IEEE Trans. Robot. Autom.*, vol. 12, no. 5 pp. 775–788, Oct. 1996.

[31] M. Garciaelias, K. AN, L. Berglund, R. Linscheid, W. Cooney, and E. Chao, "Extensor mechanism of the fingers—Part I: A quantitative geometric study," *J. Hand Surg.*, vol. 16A, no. 6, pp. 1130–1136, Nov. 1991.

[32] A. Hollister, W. L. Buford, L. M. Myers, D. J. Giurintano, and A. Novick, "The axes of rotation of the thumb carpometacarpal joint," *J. Orthopaedic Res.*, vol. 10, no. 3, pp. 454–460, May 1992.

[33] A. Hollister, D. J. Giurintano, W. L. Buford, L. M. Myers, and A. Novick, "The axes of rotation of the thumb interphalangeal and metacarpophalangeal joints," *Clin. Orthopaedic Related Res.*, vol. 320, pp. 188–193, Nov. 1995.

[34] K. Holzbaur, W. Murray, and S. Delp, "A model of the upper extremity for simulating musculoskeletal surgery and analyzing neuromuscular control," *Ann. Biomed. Eng.*, vol. 33, no. 6, pp. 829–840, 2005.

[35] Hosmer Dorrance Corporation. (2009, Sep.). Body-powered prosthetic hand. [Online]. Available: http://www.hosmer.com/products/hooks/index.html

[36] S. Jacobsen, E. Iversen, D. Knutti, R. Johnson, and K. Biggers, "Design of the Utah/M.I.T. dextrous hand," in *Proc. IEEE Int. Conf. Robot. Autom.*, Apr. 1986, vol. 3, pp. 1520–1532.

[37] A. Kargov, C. Pylatiuk, R. Oberle, H. Klosek, T. Werner, W. Roessler, and S. Schulz, "Development of a multifunctional cosmetic prosthetic hand," in *Proc. IEEE Int. Conf. Rehabil. Robot.*, 2007, pp. 550–553.

[38] J. A. Katarincic, "Thumb kinematics and their relevance to function," *Hand Clin.*, vol. 17, pp. 169–174, 2001.
[39] H. Kawasaki, T. Komatsu, and K. Uchiyama, "Dexterous anthropomorphic robot hand with distributed tactile sensor: Gifu Hand II," *IEEE/ASME Trans. Mechatronics*, vol. 7, no. 3, pp. 296–303, Sep. 2002.
[40] Kollmorgen, Inc. (2010). "Kollmorgen motors," [Online]. Available: http://www.kollmorgen.com/
[41] T. Kuiken, G. Dumanian, R. Lipschutz, L. Miller, and K. Stubblefield, " The use of targeted muscle reinnervation for improved myoelectric prosthesis control in a bilateral shoulder disarticulation amputee," *Prosthet. Orthot. Int.*, vol. 28, no. 3, pp. 245–253, Dec. 2004.
[42] M. Kumon, I. Mizumoto, Z. Iwai, and A. Indou, "Shape memory alloy actuator with simple adaptive control," presented at the 2nd Int. Conf. on Innovative Computing, Information and Control, Kumamoto, Japan, 2007.
[43] P. J. Kyberd, C. Light, P. H. Chappell, J. M. Nightingale, D. Whatley, and M. Evans, "The design of anthropomorphic prosthetic hands: A study of the Southampton Hand," *Robotica*, vol. 19, no. 6, pp. 593–600, 2001.
[44] T. Lan, Y. W. Liu, M. H. Jin, S. W. Fan, H. G. Fang, J. J. Xia, and H. Liu, "DSP and FPGA-based joint impedance controller for DLR/HIT II dexterous robot hand," in *Proc. IEEE/ASME Int. Conf. Adv. Intell. Mechatron.*, 2009, pp. 1594–1599.
[45] Liberating Technologies, Inc. (2009, Sep.), Upper extremity prosthetics. [Online]. Available: http://www.liberatingtech.com
[46] F. Lotti, P. Tiezzi, G. Vassura, L. Biagiotti, G. Palli, and C. Melchiorri, "Development of UB Hand 3: Early results," in *Proc. IEEE Int. Conf. Robot. Autom.*, Apr. 2005, pp. 4488–4493.
[47] C. Lovchik and M. Diftler, "The Robonaut hand: A dexterous robot hand for space," in *Proc. IEEE Int. Conf. Robot. Autom.*, 1999, vol. 2, pp. 907–912.
[48] Motion Control, Inc. (2009, Sep.). The motion control ETD. [Online]. Available: http://www.utaharm.com/
[49] T. Mouri, H. Kawasaki, Y. Keisuke, J. Takai, and S. Ito, "Anthropomorphic robot hand: Gifu Hand III," in *Proc. Int. Conf. Control, Autom. Syst.*, 2002, p. 1288.
[50] M. Nicolelis, "Actions from thoughts," *Nature*, vol. 409, no. 6818, pp. 403–407, Jan. 2001.
[51] D. Nishikawa, Y. Ishikawa, W. Yu, M. Maruishi, I. Watanabe, H. Yokoi, Y. Mano, and Y. Kakazu, "On-line learning based EMG prosthetic hand," presented at the Cong. of Int. Soc. of Electrophysiology and Kinesiology, Sapporo, Japan, 2000.
[52] T. Okada, "Object handling system for manual industry," *IEEE Trans. Syst., Man Cybern.*, vol. SMC-9, no. 2, pp. 79–89, Feb. 1979.
[53] OttoBock HealthCare, Inc. (2009, Sep.). Cable-controlled arm prostheses. [Online]. Available: http://www.ottobock.com
[54] RTAI. (2005). [Online]. Available: http://www.rtai.org
[55] J. K. Salisbury and J. J. Craig, "Articulated hands: Force control and kinematic issues," *Int. J. Robot. Res.*, vol. 1, pp. 4–17, 1982.
[56] V. J. Santos and F. J. Valero-Cuevas, "Anatomical variability naturally leads to multimodal distributions of Denavit–Hartenberg parameters for the human thumb," *Eng. Med. Biol. Soc.*, vol. 2, pp. 1823–1826, 2003.
[57] K. Sasaki, Y. Fujikake, H. Takahashi, and M. R. Cutkosky, "Manipulation of an object using slip sensing tactile sensor," presented at the Int. Conf. on Machine Automation—Adv. Mechatron.: First-Time-Right, Tampere, Finland, 1998.
[58] T. Senoo, Y. Yamakawa, S. Mizusawa, A. Namiki, M. Ishikawa, and M. Shimojo, "Skillful manipulation based on high-speed sensory-motor fusion," in *Proc. IEEE Int. Conf. Robot. Autom.*, May 2009, pp. 1611–1612.
[59] ShadowHand. (2010). Shadow robot company. [Online]. Available: http://www.shadowrobot.com/hand/
[60] D. H. Silcox, M. D. Rooks, R. R. Vogel, and L. L. Fleming, "Myoelectric prostheses—A long-term follow-up and a study of the use of alternate prostheses," *J. Bone Joint Surg.—Amer. Volume*, vol. 75A, pp. 1781–1789, 1993.
[61] W. P. Smutz, A. Kongsayreepong, R. E. Hughes, G. Niebur, W. P. Cooney, and K. N. An, "Mechanical advantage of the thumb muscles," *J. Biomechan.*, vol. 31, pp. 565–570, 1998.
[62] T. H. Speeter, "Primitive based control of the UTAH/MIT hand," in *Proc. Int. Conf. Robot. Autom.*, 1991, pp. 866–877.
[63] S. Sueda, A. Kaufman, and D. Pai, "Musculotendon simulation for hand animation," in *Proc. ACM SIGGRAPH*, 2008, pp. 1–8.
[64] Touch Bionics, Inc. (2009, May). Fitting and service manual. [Online]. Available: http://www.touchbionics.com/
[65] W. Townsend, "The Barrett hand grasper—Programmably flexible part handling and assemble," *Int. J. Ind. Robot*, vol. 27, no. 3, pp. 181–188, 2000.
[66] W. Tsang, K. Singh, and E. Fiume, "Helping hand: An anatomically accurate inverse dynamics solution for unconstrained hand motion," in *Proc. ACM SIGGRAPH/Eurograph. Symp. Comput. Animat.*, 2005, pp. 319–328.
[67] T. Tsuji, S. Miyata, T. Hashimoto, and H. Kobayashi, "Controller design for robot with pneumatic artificial muscles," in *Proc. Int. Joint Conf. SICE–ICASE*, 2006, pp. 5419–5422.
[68] J. Ueda, Y. Ishida, M. Kondo, and T. Ogasawara, "Development of the NAIST-Hand with vision-based tactile fingertip sensor," in *Proc. IEEE Int. Conf. Robot. Autom.*, Apr. 2005, pp. 2332–2337.
[69] M. V. Weghe, M. Rogers, M. Weissert, and Y. Matsuoka, "The ACT hand: Design of the skeletal structure," in *Proc. IEEE Int. Conf. Robot. Autom.*, 2004, pp. 3375–3379.
[70] M. Velliste, S. Perel, M. C. Spalding, A. S. Whitford, and A. B. Schwartz, "Cortical control of a prosthetic arm for self-feeding," *Nature*, vol. 453, no. 7198, pp. 1098–1101, Jun. 2008.
[71] S. Wakimoto, K. Suzumori, and T. Kanda, "Development of intelligent mckibben actuator," in *Proc. IEEE/RSJ Int. Conf. Intell. Robots Syst.*, 2005, pp. 487–492.
[72] D. Wilkinson, M. Vande Weghe, and Y. Matsuoka, "An extensor mechanism for an anatomical robotic hand," in *Proc. IEEE Int. Conf. Robot. Autom.*, Sep. 2003, pp. 238–243.
[73] Z. Xu, T. Deyle, and C. Kemp, "1000 Trials: An empirically validated end effector that robustly grasps objects from the floor," in *Proc. IEEE Int. Conf. Robot. Autom.*, May 2009, pp. 2160–2167.
[74] I. Yamano and T. Maeno, "Five-fingered robot hand using ultrasonic motors and elastic elements," in *Proc. IEEE Int. Conf. Robot. Autom.*, Apr. 2005, pp. 2673–2678.
[75] F. E. Zajac, "Muscle coordination of movement: A perspective," *J. Biomech.*, vol. 26, no. 1 (suppl.), pp. 109–124, 1993.

Ashish D. Deshpande received the Ph.D. degree in mechanical engineering from the University of Michigan, Ann Arbor, in 2007.

He is currently an Assistant Professor in the Mechanical Engineering Department, University of Texas, Austin. He was a Research Associate in the NeuRobotics Laboratory, University of Washington, Seattle. His current research interests include development of new methodologies to represent full dynamics of general robotic systems, design and development of search and rescue robot teams, and implementation of robotics methods for human motion modeling and design of prostheses; development of robot devices based on biomechanical analyses to assist in rehabilitation and to improve prostheses design; study of neuromuscular controls in humans to implement human-like motion and force controls in anatomical robotic systems; and study of the dynamics and controls of multi-body robotic systems and their application to human motion analysis.

Dr. Deshpande was the recipient of an NSF CAREER Award.

Zhe (Joseph) Xu received the B.S. degree (with university honors) from China Agricultural University, Beijing, China, in 2004, and the M.S. degree from the University of Hawaii, Manoa, in 2007, both in mechanical engineering. He is currently working toward the Ph.D. degree in the Computer Science and Engineering Department, University of Washington, Seattle.

He is a former member of the Healthcare Robotics Laboratory at the Georgia Institute of Technology.

Mr. Zhu earned the First Prize in the 2nd Undergraduate Mechanical Innovation Contest in China in 2004.

Michael J. Vande Weghe received the S.B.E.E. degree from the Massachusetts Institute of Technology, Cambridge, in 1990, and the M.S. degree in robotics from Carnegie Mellon University (CMU), Pittsburgh, PA, in 2002.

He is currently a Senior Research Engineer in The Robotics Institute, Carnegie Mellon University, Pittsburgh, PA, where he is responsible for the mechanical, electrical, and driver-level software systems for the Active Home project. As the Principal Engineer for the ACT Hand from 2002 to 2008, he designed and built several versions of the ACT Hand. His past experience includes small-scale actuator design, distributed systems software development, real-time speech recognition research, and high-frequency power electronics design.

Benjamin H. Brown received the B.S. and M.S. degrees in mechanical engineering from Carnegie Mellon University, Pittsburgh, PA, in 1967 and 1976, respectively.

He is currently a Project Scientist at The Robotics Institute, Carnegie Mellon University, Pittsburgh, PA, with more than 25 years of experience in the robotics field. He is interested in the analysis and design of robots and electromechanical systems, and specializes in the development of high-performance structures and devices, dynamically stabilized robots in particular. He has worked on a wide variety of robotics projects, including wheeled, tracked and legged vehicles, as well as snake-like devices, for space and terrestrial applications. Current projects include a ruggedized snake robot for rough-terrain and underwater locomotion; a dynamic, legged climbing (Parkour) robot; reconfigurable, modular cubical robot (Claytronics); and conversion of passenger cars to electric power (ChargeCar). He is the holder of three patents and has authored or coauthored more than 50 conference and journal papers, mainly in the field of mobile robotics.

Jonathan Ko received the Ph.D. degree from the Department of Computer Science, University of Washington, Seattle, in 2011. His research was focused on machine learning for robotic systems, in particular, Gaussian processes for modeling of dynamical systems.

He is currently with Google, Inc., Seattle, WA.

Dr. Ko was a recipient of the Sarcos Best Student Paper Award at the Conference of Intelligent Robots and Systems (IROS 2007).

Lillian Y. Chang received the Ph.D. degree in robotics from Carnegie Mellon University, Pittsburgh, PA.

She is a 2010 Computing Innovation Fellow (CIFellow), funded through a National Science Foundation grant to the Computing Community Consortium (CCC) within the Computing Research Association (CRA). She is hosted by Intel Corporation and is also a Research Associate at the University of Washington, Seattle. Her research interests include dexterous manipulation and motion planning, quality-of-life applications of robotics, and interfaces for human–robot interaction.

Dr. Chang is a former NASA Harriet G. Jenkins Pre-doctoral Fellow and a former NSF Graduate Research Fellow.

David D. Wilkinson received the B.S. degree in engineering from The Johns Hopkins University, Baltimore, MD, and the M.S. degree from Carnegie Mellon University, Pittsburgh, PA, in 1992 and 2002, respectively.

He has more than 16 years experience working in industry and academia as an engineer, project manager, and engineering director. In 2002, while working towards his Master's degree at Carnegie Mellon, he was awarded a full-year scholarship through the Siebel Scholar program. He has spent the last five years working at Barrett Technology, Cambridge, MA. Barrett Technology is a leader in advanced robotic manipulators. As the Director of Engineering, he manages a small team of engineers and numerous ongoing R&D projects covering all aspects of robotic technology including mechanics, electronics, and software. Previous to his employment at Barrett Technology, he worked as a self-employed engineering consultant for over a year. Prior to this, he spent two years as an Engineer at BF Goodrich Aerospace, designing and testing hardware for military helicopters. The first five years of his engineering career were spent as an engineer designing, developing, and testing medical and optical equipment for the GSI Group, including an advanced holographic printing machine for the medical industry.

Sean M. Bidic received the B.S. and B.A. degrees in behavior and health care systems management from the Wharton School of Business, University of Pennsylvania, Philadelphia. He received the Ph.D. degree in medicine from the College of Physicians and Surgeons, Columbia University, New York, NY, and completed an integrated plastic surgery residency at the University of Pittsburgh, Pittsburgh, PA.

During his general and plastic surgery training, he was a Research Fellow at the Institute for Complex Engineered Systems and The Robotics Institute, Carnegie Mellon University, Pittsburgh, PA. During this time, he also completed a Master's degree in fine arts at the School of Art, Carnegie Mellon University. He recently completed a hand and microsurgery fellowship, while serving as a Clinical Instructor in orthopedics surgery at the University of California, Los Angeles. He is elated to join the faculty at The University of Texas Southwestern Clinical Procedure Center, Dallas, and to serve not only UT but the Dallas/Fort Worth community as well. His research interests include interdisciplinary investigations and exploring and developing intersections between art and medicine. He is also involved in many research projects focused on constructing a robotic upper extremity and developing synthetic bone substitutes.

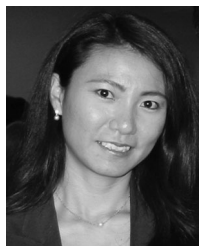

Yoky Matsuoka received the B.S. degree in electrical engineering and computer sciences (EECS) from the University of California, Berkeley, in 1993. She received the M.S. degree in EECS and the Ph.D. degree in EECS in the fields of artificial intelligence and computational neuroscience in 1995 and 1998, respectively, both from Massachusetts Institute of Technology, Cambridge.

Currently, she is the Torode Family Endowed Professor in the Department of Computer Science and Engineering, University of Washington, Seattle.

Dr. Matsuoka received the Presidential Early Career Award for Scientists and Engineers (PECASE) in 2004, the Anna Loomis McCandless Chair in 2004, the IEEE Robotics and Automation Society Early Academic Career Award in 2005, and was a MacArthur Foundation Fellow in 2007.